





## Scale-free localization and $\mathcal{PT}$ symmetry breaking from local non-Hermiticity

Bo Li , He-Ran Wang , Fei Song , and Zhong Wang 

*Institute for Advanced Study, Tsinghua University, Beijing 100084, China*



(Received 13 February 2023; accepted 27 September 2023; published 18 October 2023)

We show that a local non-Hermitian perturbation in a Hermitian lattice system generically induces scale-free localization for the continuous-spectrum eigenstates. When the perturbation lies at a finite distance to the boundary, the scale-free eigenstates are promoted to exponentially localized modes, whose number is proportional to the distance. Furthermore, when the local non-Hermitian perturbation respects parity-time ( $\mathcal{PT}$ ) symmetry, the  $\mathcal{PT}$  symmetry breaking is always accompanied by the emergence of scale-free or exponential localization. Intriguingly, we find a concise band-structure condition which tells not only when the continuous-spectrum  $\mathcal{PT}$  breaking of scale-free modes can occur but also the precise  $\mathcal{PT}$ -breaking energy window. Our results uncover a series of unexpected generic phenomena induced by a local non-Hermitian perturbation, which has interesting interplay with  $\mathcal{PT}$  symmetry.

DOI: [10.1103/PhysRevB.108.L161409](https://doi.org/10.1103/PhysRevB.108.L161409)

**Introduction.** Non-Hermiticity of a Hamiltonian often arises in open or nonequilibrium systems [1,2]. It induces remarkable phenomena such as unidirectional invisibility [3,4], single-mode lasing [5,6], and enhanced sensitivity [7–10]. Many of them are related to the parity-time ( $\mathcal{PT}$ ) symmetric Hamiltonians, which generally have two phases when their parameters are varied, namely, the  $\mathcal{PT}$ -exact and  $\mathcal{PT}$ -broken phases, for which the eigenenergies are real and complex, respectively [11–15]. They are bridged by the  $\mathcal{PT}$ -breaking transition at the exceptional points (EPs).

Recently, progress in non-Hermitian topological phases has revealed the non-Hermitian skin effect (NHSE) [16–26], the aggregation of eigenstates near boundaries, which underlines a striking modification of bulk-boundary correspondence in non-Hermitian systems. Whereas NHSE stems from the non-Hermiticity of the entire system, another common scenario in non-Hermitian physics is that the system is subject to local non-Hermiticity. For example, it is often the case that the gain or loss occurs only at the boundaries, preserving the Hermiticity of the bulk system [27–34]. The system can be modeled by a Hermitian Hamiltonian with local non-Hermitian terms.

In this letter, we show that, in one-dimensional Hermitian lattice systems, local non-Hermiticity at boundaries generally gives rise to a scale-free localization, for which the spatial decay length of eigenstates is proportional to the system size, such that the eigenstates retain the same profiles if the system size is taken as the measure of length. The phenomenon is robust and generic. As such, it fundamentally differs from the scale-free NHSE under global non-Hermiticity, which requires fine tuning certain parameters [35–37]. More surprisingly, when the local non-Hermiticity is located at a finite distance to boundary, it also brings about a collection of bound states that exponentially localize to the impurity. The localization length and population of bound modes rely on the distance but are independent of the system size. Furthermore, when the local non-Hermiticity respects  $\mathcal{PT}$  symmetry, we find that the emergence of scale-free or bound states always

coincides with  $\mathcal{PT}$  breaking. Unexpectedly, the  $\mathcal{PT}$  breaking associated with scale-free modes under open boundary conditions (OBC) is dictated by a simple band-structure-based criterion, which also tells the energy window of  $\mathcal{PT}$  breaking.

*Scale-free localization from local non-Hermitian perturbation.* To be concrete, we start with a simple model:

$$H = \sum_{j=1}^{L-1} t(|j\rangle\langle j+1| + |j+1\rangle\langle j|) + ig|1\rangle\langle 1|, \quad (1)$$

where the first two terms describe nearest hopping with a real parameter  $t$ , the last term represents a boundary gain controlled by  $g$ . OBC has been built in the Hamiltonian. Let an eigenstate be  $|\psi\rangle = \sum_j \psi_j |j\rangle$ , then the eigenequation in the bulk reads  $t(\psi_{j-1} + \psi_{j+1}) = E\psi_j$ , whose characteristic equation is given by  $t(\beta + \beta^{-1}) = E$ . This allows the eigenstate ansatz:

$$\psi_j(\beta) = c_1 \beta^j + c_2 \beta^{-j}, \quad (2)$$

where  $c_1, c_2$  are coefficients determined by boundary conditions. Applying the ansatz to the real-space eigenequation  $H|\psi(\beta)\rangle = E|\psi(\beta)\rangle$ , OBC results in a zero determinant condition:

$$\det \begin{bmatrix} ig\beta - t & ig\beta^{-1} - t \\ t\beta^{L+1} & t\beta^{-(L+1)} \end{bmatrix} = 0. \quad (3)$$

The spectrum of the Hamiltonian Eq. (1) is complex [Fig. 1(a)], which demands nonunitary solutions, i.e.,  $|\beta| \neq 1$ , since  $|\beta| = 1$  always gives real eigenvalues. If  $|\beta|^L \gg 1$  for a large system ( $L \gg 1$ ), Eq. (3) reduces to  $t\beta^{L+1}(ig\beta^{-1} - t) = 0$ , which could be satisfied by a bound state solution  $\beta \simeq ig/t$  when  $|g| > t$ ; the case for  $|\beta|^L \ll 1$  is similar. However, the Hamiltonian has  $L$  eigenvalues; thus, the rest of the solutions should scale as  $|\beta|^L \sim O(1)$  even for  $L \gg 1$ . Therefore, to the leading order of  $L^{-1}$ , the solution approximately satisfies

$$|\beta| \simeq e^{c/L}, \quad (4)$$

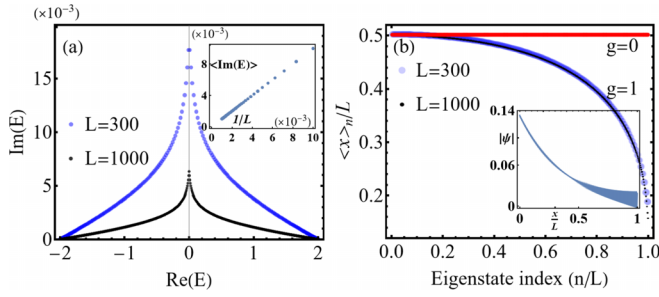


FIG. 1. Scale-free localization for model Eq. (1). (a) Eigenvalues in the complex plane with  $g = 1$ . The inset shows the averaged imaginary part of energy  $\langle \text{Im}(E) \rangle$  for varying  $1/L$ . (b) Eigenvalue-resolved mean positions. The eigenstate index is arranged in the ascending order of the eigenvalue imaginary part. The inset gives a typical wave function profile exhibiting scale-free localization. For (a) and (b),  $t = 1$ .

where  $c$  is size independent (it is generally eigenstate dependent), so that  $|\beta|^L = e^c \sim O(1)$ . This displays a scale-free localization, i.e., the decay length is proportional to the system size. The (right) eigenstate profile respects a scale invariance  $|\psi_L(x)| \simeq e^{cx/L} \simeq |\psi_{sL}(sx)|$ , with  $s$  being a scaling factor. This feature can be further demonstrated by a eigenvalue-resolved mean position  $\langle x \rangle_n = \sum_{j=1}^L |\psi_{n,j}|^2 j / \sum_{j=1}^L |\psi_{n,j}|^2$ . As plotted in Fig. 1(b),  $\langle x \rangle_n$  for the non-Hermitian case ( $g = 1$ ) deviates from the uniform distribution ( $g = 0$ ), and the curve shows a perfect self-similarity upon varying system size (with appropriately scaling the coordinates and eigenvalue index). In addition, it is evident that the imaginary part of eigenvalues are proportional inversely to the system size  $L$  because  $\text{Im}E \propto |\beta| - |\beta^{-1}| \approx 2c/L$ , which agrees with Fig. 1(a). From our analysis, it is clear that the scale-free localization is a generic consequence of a local non-Hermitian perturbation to a Hermitian lattice Hamiltonian [38,39].

*Accumulation of bound states.* Moving the position of the non-Hermitian impurity away from the boundary, we unveil another interesting consequence: Aside from scale-free modes, a local (even single-site) non-Hermitian impurity can induce an arbitrary number of exponentially localized modes. The localization length ( $\xi_{\text{loc}}$ ) and population of these modes depend on the distance between the impurity and the boundary but not on the system size. For concreteness, we replace the non-Hermitian term in the model in Eq. (1) by  $ig|d\rangle\langle d|$ , meaning that the distance between impurity and boundary is  $d$ . The insets in Fig. 2(a) show that there are a bunch of eigenmodes aggregating to the impurity, and they have a size-independent imaginary part of the eigenvalues (isolated from the continuous spectrum) and localization length. Like the case of Eq. (1), the eigenvalues here follow  $E = t(\beta + \beta^{-1})$ , while the eigenstate wave function takes the general form:  $|\psi\rangle = \sum_{1 \leq j < d} \psi_j^{(1)} |j\rangle + \sum_{d \leq j \leq L} \psi_j^{(2)} |j\rangle$ , with  $\psi_j^{(v)} = a_v \beta^j + b_v \beta^{-j}$  ( $v = 1, 2$ ). By adapting the bulk equation to the boundary and the impurity in the thermodynamic limit ( $L \rightarrow \infty$ , but  $1 \ll d \ll L$ ), we obtain the equation for localized modes:

$$ig\beta^{2d+1} - t\beta^2 - ig\beta + t = 0, \quad (5)$$

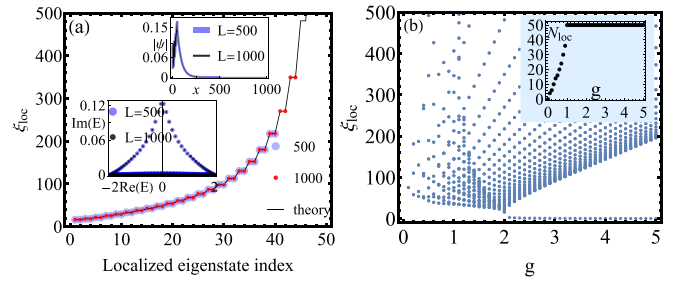


FIG. 2. (a) Localization length extracted from exactly diagonalized wave function and theory, where only  $\xi_{\text{loc}} \leq 500$  is shown; the insets show exemplified eigenvalues and eigenstate profile for different system size.  $t = 1$ ,  $d = 50$ , and  $g = 2$  are used. (b) Localization length ( $\xi_{\text{loc}} \leq 500$ ) and the number of bound states (the inset) as a function of impurity strength  $g$ ,  $t = 1$ ,  $d = 50$ .

in which  $|\beta| < 1$  is imposed to ensure the states being piled up to the impurity. Numerically solving this equation (taking  $d = 50$ ), we obtain  $d$  localized modes, whose localization lengths agree well with that ( $\xi_{\text{loc}} = 1/|\ln|\beta||$ ) extracted from eigenstate wave functions for  $L = 500$  and  $1000$ , as shown in Fig. 2. Moreover, Fig. 2(b) shows that, while varying the strength of impurity can substantially affect the localization length, the exponential localization is obtained for a wide range of  $g$ .

Notably, exponentially localized modes from Eq. (5) can be viewed as scale-free modes with respect to the subsystem between the boundary and impurity, given that the localization length is comparable with the length of the subsystem:  $|\beta| \sim e^{c/d}$ . Meanwhile, they are exponentially localized modes for the whole system since  $d \ll L$ . Moreover, the localized modes arising from local non-Hermiticity here differ sharply from the Hermitian counterpart [by removing  $i$  in Eq. (5)], where only a few localized modes are obtained (not proportional to  $d$ ).

*$\mathcal{PT}$  breaking and localization.* We now show that, if a system with local non-Hermitian perturbation respects  $\mathcal{PT}$  symmetry, an intriguing interplay arises between  $\mathcal{PT}$  breaking and scale-free (or exponential) localization. Let us consider a  $\mathcal{PT}$ -symmetric Hamiltonian  $H = H_0 + V$ , where  $V$  is a local non-Hermitian perturbation lying at or near the boundaries, and  $H_0$  is a one-dimensional (1D) Hermitian chain with  $L$  sites. Specifically,  $H_0$  contains  $n$ th nearest-neighbor hopping with parameter  $t_n (\in \mathbb{C})$  and can be well adapted to periodic boundary conditions (PBC) or OBC. To solve the eigenstates and eigenvalues, one takes the wave function ansatz  $\psi_j = \sum_{\mu=1}^{2M} c_\mu \beta_\mu^j$  ( $c_\mu$  takes different values for intervals partitioned by in-bulk impurities), where  $\beta_\mu$  satisfies the characteristic equation  $E = \sum_{n=1}^M t_n \beta^n + t_n^* \beta^{-n}$ , with the same energy  $E$ . Legitimate  $E$  is determined by the boundary condition and/or eigenequations near impurities. In the  $\mathcal{PT}$ -exact phase, we know *a priori* that  $E$  must be real, so that at least two of the corresponding  $\beta_\mu$ 's are on the unit circle, i.e.,  $\beta = e^{ik}$  with real momentum  $k$ , and their contributions dominate the wave function in the bulk [40]. The real-valuedness of  $E$  dictates that  $V$  cannot drag  $\beta$  away from the unit circle, and therefore, the eigenstates remain extended (see Ref. [41] for more details). In the  $\mathcal{PT}$ -broken phase, however, com-

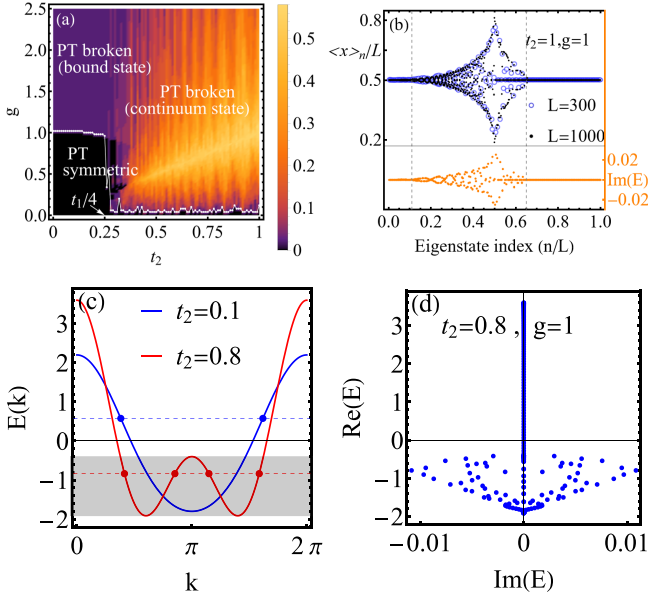


FIG. 3. (a) Phase diagram for an open chain driven by boundary gain and loss. The color map shows  $P_{\text{com}}$ . The system size is  $L = 100$ . (b) The eigenvalue-resolved mean position  $\langle x \rangle_n/L$  (upper, left ticks, black) and the imaginary part of eigenvalue (lower, right ticks, orange), where band index is arranged in the ascending order of eigenvalue real part. (c) Band structure of  $H_0$ . When  $t_2 > t_1/4$ , the curve has two local minima and the shadow region covers the energy range that allows  $\mathcal{PT}$  breaking. (d) Eigenvalues in complex plane (with  $L = 100$ ). The real parts of complex eigenvalues fall into the shadowed energy range in (c). In all plots,  $t_1 = 1$ .

plex energies enforce  $|\beta| \neq 1$ , which corresponds to either a scale-free or bound state. Therefore, we conclude that the  $\mathcal{PT}$  symmetry breaking arising from local non-Hermiticity is always accompanied by the emergence of scale-free or (and) exponential localization.

*$\mathcal{PT}$ -breaking criterion under OBC.* Furthermore, we find that  $\mathcal{PT}$  breaking associated with the scale-free modes, referred to as continuous-spectrum  $\mathcal{PT}$  breaking, has an unexpected interplay with boundary conditions. It turns out that the continuous-spectrum  $\mathcal{PT}$  breaking due to boundary non-Hermiticity occurs under PBC if the perturbation is strong enough [41]. In sharp contrast, we find that, under OBC, the (unperturbed) band structure dictates the  $\mathcal{PT}$  breaking.

We state the conclusion first: For an open chain with band structure given by  $\{E_n(k)\}$  (single or multiple band) in momentum space, the  $\mathcal{PT}$  symmetry breaking (of a continuous spectrum) arising from boundary non-Hermiticity can only take place at energies with more than one pair of equal-energy points. For instance,  $\mathcal{PT}$  breaking can occur for the system with the red band curve in Fig. 3(c) in the shadowed energy window, where four equal-energy points exist, while it is prohibited for the blue band curve, as only two equal-energy points exist.

We demonstrate the mechanism in the following by assuming the single band, though extension to multiband cases is straightforward. The physics can be understood by investigating the formation of EPs during  $\mathcal{PT}$  breaking, which requires the coalescence of at least two eigenenergies, see

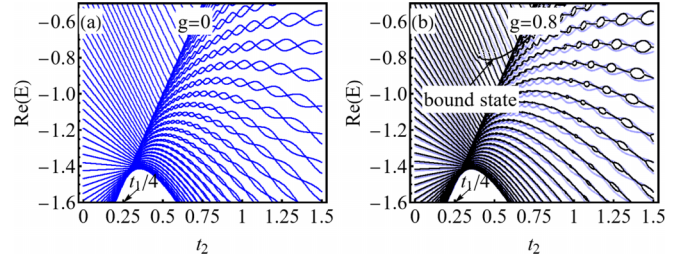


FIG. 4. Spectrum for model described by Eqs. (6) and (7). (a) The Hermitian case. (b) The real part of non-Hermitian spectrum (black) with  $g = 0.8$ , overlapped with Hermitian spectrum (blue). The  $\mathcal{PT}$  breaking occurring between bound states is marked.  $t_1 = 1$  and  $L = 100$  are fixed.

Fig. 4. The eigenvalue is still real-valued at EP, so that it can be captured by the band structure  $E(k)$ , where the value of  $k$  is determined by the local perturbation and boundary condition. Due to the energy degeneracy at EP, the band structure at  $E(k) = \varepsilon_{\text{EP}}$  should be able to hold at least two eigenmodes, such that they develop a Jordan block at EP. The eigenstates under OBC are standing waves composed of forward and backward plane wave, i.e., for a given energy  $\varepsilon$ ,  $\psi_{\text{OBC}}(x) \sim c_1 e^{ik_1 x} + c_2 e^{-ik_2 x}$  with  $E(k_1) = E(-k_2) = \varepsilon$ . Thus, only one OBC eigenmode can be constructed from two real solutions of the equation  $E(k) = \varepsilon$ , which manifests as the absence of eigenvalue degeneracy (e.g., see the spectrum for  $t_2 < t_1/4$  in Fig. 4). Therefore, EP can never exist at an energy with only one pair of equal-energy points, where only one eigenmode is allowed. In contrast, in the presence of more than one pair of equal-energy points, at least two eigenstates of the same energy exist, which enables EP formation.

As a comparison, the PBC case [41] is different in the sense that each equal-energy point represents an independent plane-wave eigenmode  $\psi_{\text{PBC}}(x) \sim e^{ikx}$ , which allows EP formation from two equal-energy points. Note that our statement does not apply to isolated bound states, which are not captured by band structure  $E(k)$  with real  $k$ .

According to our criterion, a single-band system with only nearest-neighbor hopping, whose band structure looks like the blue one in Fig. 3(c), cannot have continuous-spectrum  $\mathcal{PT}$  breaking under OBC, in stark contrast with the PBC behavior [41]. This motivates us to consider a model with second-nearest-neighbor hopping:

$$H_0 = \sum_{j=1}^{L-1} t_1 |j\rangle \langle j+1| + \sum_{j=1}^{L-2} t_2 |j\rangle \langle j+2| + \text{H.c.}, \quad (6)$$

where  $t_1, t_2$  are real and positive, and the non-Hermitian boundary potential  $V$  is given by

$$V = ig(|1\rangle \langle 1| - |L\rangle \langle L|). \quad (7)$$

The phase diagram is plotted in Fig. 3(a), where the  $\mathcal{PT}$  breaking is quantified by the proportion of complex eigenvalues  $P_{\text{com}} = n_{\text{com}}/L$ , with  $n_{\text{com}}$  being the number of complex eigenvalues. The  $\mathcal{PT}$  breaking of the continuous spectrum is prohibited until  $t_2 > t_1/4$  because the band structure has one local minimum for  $t_2 < t_1/4$ , thus only allows one pair of equal-energy points. Figure 3(c) gives two representative

cases, where the red curve fulfills the requirement and the shadow region marks the allowed energy window for  $\mathcal{PT}$  breaking. As shown in (d), the energy real part of  $\mathcal{PT}$ -broken modes precisely falls into this range. In addition, we confirmed the correspondence between  $\mathcal{PT}$  breaking and scale-free localization in Fig. 3(b), where the eigenvalue-resolved mean position only shows deviation from middle position for  $\mathcal{PT}$ -broken modes. It is also worth noting that there are two  $\mathcal{PT}$ -broken modes (even for  $t_2 < t_1/4$ ) stemming from isolated bound states near boundaries if the non-Hermitian term is large enough, irrespective of the criterion for continuous spectrum.

The real part of the spectrum in Fig. 4(d) shows that the  $\mathcal{PT}$  breaking takes place by deforming nearest real energy levels into complex ones through an EP, which stimulates an intuitive understanding by projecting the Hamiltonian into two-level subspaces. The model in Eq. (6) is inversion symmetric, so that its eigenstates can be categorized with even or odd parity. Under OBC, accidental degeneracy in the spectrum [Fig. 4(a)] can exist for modes with opposite parity [41]. In a subspace effective theory, the perturbation  $V$  can only couple modes belonging to opposite parities, as it is inversion antisymmetric, i.e.,  $\mathcal{P}V\mathcal{P} = -V$ , with  $\mathcal{P}$  being the inversion operator; hence, the perturbative terms in the effective Hamiltonian are off-diagonal and anti-Hermitian. The effective Hamiltonian for two eigenmodes involved in a  $\mathcal{PT}$  breaking takes the form:

$$H_{\text{eff}} = \Delta_{12}\sigma_z + ig(d_x\sigma_x + d_y\sigma_y), \quad (8)$$

where  $\Delta_{12}$  represents the energy gap, and  $d_x, d_y$  are functions of the involved modes and the perturbation. At the degenerate point  $\Delta_{12} = 0$ , the eigenvalue of the effective Hamiltonian is  $\pm ig\sqrt{d_x^2 + d_y^2}$ , namely, the  $\mathcal{PT}$  symmetry is broken if  $g \neq 0$ , agreeing with the vanishing threshold in Fig. 3(a) (in the  $t_2 > t_1/4$  regime). Here, one should notice that the

vanishing  $\mathcal{PT}$ -breaking threshold is attributed to the inversion antisymmetry of perturbation, which can couple equal-energy modes of opposite parity. When an inversion symmetric non-Hermitian perturbation is considered, it would mix gapped modes belonging to the same parity. The perturbation needs to be strong enough to overcome the gap, which corresponds to a finite threshold [41].

*Conclusions.* We show that a local non-Hermitian perturbation in Hermitian lattices can generically induce scale-free localization for continuous-spectrum eigenstates. Furthermore, the same mechanism can generate a collection of exponentially localized modes when the local non-Hermitian perturbation sits at a finite distance to the boundary, and the number of these modes is proportional to the distance. When  $\mathcal{PT}$  symmetry is present, we show that the scale-free localization emerges simultaneously with the  $\mathcal{PT}$  breaking. The continuous-spectrum  $\mathcal{PT}$  breaking (associated with scale-free modes) arising from local boundary perturbation is dictated by a concise criterion based on band structure.

One of the most promising platforms for verifying our results is optics systems, where gain and loss can be conveniently controlled, based on which tremendous progress on  $\mathcal{PT}$  symmetric non-Hermitian physics has been achieved [42–48]. Another promising setup is an array of cavities, which plays important roles in studying driven-dissipative quantum systems [49–53]. Its inherent non-Hermiticity can be engineered according to our proposals. Our results are also relevant to other boundary-driven/dissipated systems. As a final remark, it will be interesting to generalize our results to many-body systems; for example, the XXZ spin chain subject to a  $\mathcal{PT}$ -symmetric imaginary magnetic field on boundaries for which integrable techniques based on the Bethe ansatz are available [54,55].

*Acknowledgment.* This letter is supported by NSFC under Grant No. 12125405.

- 
- [1] Y. Ashida, Z. Gong, and M. Ueda, Non-Hermitian physics, *Adv. Phys.* **69**, 249 (2020).
- [2] M. M. Sternheim and J. F. Walker, Non-Hermitian Hamiltonians, decaying states, and perturbation theory, *Phys. Rev. C* **6**, 114 (1972).
- [3] Z. Lin, H. Ramezani, T. Eichelkraut, T. Kottos, H. Cao, and D. N. Christodoulides, Unidirectional invisibility induced by  $\mathcal{PT}$ -symmetric periodic structures, *Phys. Rev. Lett.* **106**, 213901 (2011).
- [4] L. Feng, Y.-L. Xu, W. S. Fegadolli, M.-H. Lu, J. E. B. Oliveira, V. R. Almeida, Y.-F. Chen, and A. Scherer, Experimental demonstration of a unidirectional reflectionless parity-time metamaterial at optical frequencies, *Nat. Mater.* **12**, 108 (2013).
- [5] H. Hodaei, M.-A. Miri, M. Heinrich, D. N. Christodoulides, and M. Khajavikhan, Parity-time-symmetric microring lasers, *Science* **346**, 975 (2014).
- [6] L. Feng, Z. J. Wong, R.-M. Ma, Y. Wang, and X. Zhang, Single-mode laser by parity-time symmetry breaking, *Science* **346**, 972 (2014).
- [7] H. Hodaei, A. U. Hassan, S. Wittek, H. Garcia-Gracia, R. El-Ganainy, D. N. Christodoulides, and M. Khajavikhan, Enhanced sensitivity at higher-order exceptional points, *Nature (London)* **548**, 187 (2017).
- [8] P.-Y. Chen and J. Jung,  $\mathcal{PT}$  symmetry and singularity-enhanced sensing based on photoexcited graphene metasurfaces, *Phys. Rev. Appl.* **5**, 064018 (2016).
- [9] Z.-P. Liu, J. Zhang, Ş. K. Özdemir, B. Peng, H. Jing, X.-Y. Lü, C.-W. Li, L. Yang, F. Nori, and Y.-X. Liu, Metrology with  $\mathcal{PT}$ -symmetric cavities: Enhanced sensitivity near the  $\mathcal{PT}$ -phase transition, *Phys. Rev. Lett.* **117**, 110802 (2016).
- [10] P.-Y. Chen, M. Sakhdari, M. Hajizadegan, Q. Cui, M. M.-C. Cheng, R. El-Ganainy, and A. Alù, Generalized parity-time symmetry condition for enhanced sensor telemetry, *Nat. Electron.* **1**, 297 (2018).
- [11] C. M. Bender and S. Boettcher, Real spectra in non-Hermitian Hamiltonians having  $\mathcal{PT}$  symmetry, *Phys. Rev. Lett.* **80**, 5243 (1998).

- [12] C. M. Bender, Making sense of non-Hermitian Hamiltonians, *Rep. Prog. Phys.* **70**, 947 (2007).
- [13] Ş. K. Özdemir, S. Rotter, F. Nori, and L. Yang, Parity–time symmetry and exceptional points in photonics, *Nat. Mater.* **18**, 783 (2019).
- [14] R. El-Ganainy, K. G. Makris, M. Khajavikhan, Z. H. Musslimani, S. Rotter, and D. N. Christodoulides, Non-Hermitian physics and  $\mathcal{PT}$  symmetry, *Nat. Phys.* **14**, 11 (2018).
- [15] M.-A. Miri and A. Alù, Exceptional points in optics and photonics, *Science* **363**, eaar7709 (2019).
- [16] S. Yao and Z. Wang, Edge states and topological invariants of non-Hermitian systems, *Phys. Rev. Lett.* **121**, 086803 (2018).
- [17] S. Yao, F. Song, and Z. Wang, Non-Hermitian Chern bands, *Phys. Rev. Lett.* **121**, 136802 (2018).
- [18] F. K. Kunst, E. Edvardsson, J. C. Budich, and E. J. Bergholtz, Biorthogonal bulk–boundary correspondence in non-Hermitian systems, *Phys. Rev. Lett.* **121**, 026808 (2018).
- [19] C. H. Lee and R. Thomale, Anatomy of skin modes and topology in non-Hermitian systems, *Phys. Rev. B* **99**, 201103(R) (2019).
- [20] S. Longhi, Probing non-Hermitian skin effect and non-Bloch phase transitions, *Phys. Rev. Res.* **1**, 023013 (2019).
- [21] T. Helbig, T. Hofmann, S. Imhof, M. Abdelghany, T. Kiessling, L. W. Molenkamp, C. H. Lee, A. Szameit, M. Greiter, and R. Thomale, Generalized bulk–boundary correspondence in non-Hermitian topoelectrical circuits, *Nat. Phys.* **16**, 747 (2020).
- [22] L. Xiao, T. Deng, K. Wang, G. Zhu, Z. Wang, W. Yi, and P. Xue, Non-Hermitian bulk–boundary correspondence in quantum dynamics, *Nat. Phys.* **16**, 761 (2020).
- [23] V. M. Martínez Alvarez, J. E. Barrios Vargas, and L. E. F. Foa Torres, Non-Hermitian robust edge states in one dimension: Anomalous localization and eigenspace condensation at exceptional points, *Phys. Rev. B* **97**, 121401(R) (2018).
- [24] A. Ghatak, M. Brandenbourger, J. van Wezel, and C. Coullais, Observation of non-Hermitian topology and its bulk–edge correspondence in an active mechanical metamaterial, *Proc. Natl. Acad. Sci. USA* **117**, 29561 (2020).
- [25] W. Wang, X. Wang, and G. Ma, Non-Hermitian morphing of topological modes, *Nature (London)* **608**, 50 (2022).
- [26] E. J. Bergholtz, J. C. Budich, and F. K. Kunst, Exceptional topology of non-Hermitian systems, *Rev. Mod. Phys.* **93**, 015005 (2021).
- [27] G. T. Landi, D. Poletti, and G. Schaller, Non-equilibrium boundary driven quantum systems: Models, methods and properties, *Rev. Mod. Phys.* **94**, 045006 (2022).
- [28] F. Roccati, G. M. Palma, F. Ciccarello, and F. Bagarello, Non-Hermitian physics and master equations, *Open Syst. Inf. Dyn.* **29**, 2250004 (2022).
- [29] J. Wiersig, Role of nonorthogonality of energy eigenstates in quantum systems with localized losses, *Phys. Rev. A* **98**, 052105 (2018).
- [30] H. Fröml, C. Muckel, C. Kollath, A. Chiocchetta, and S. Diehl, Ultracold quantum wires with localized losses: Many-body quantum Zeno effect, *Phys. Rev. B* **101**, 144301 (2020).
- [31] V. Alba and F. Carollo, Noninteracting fermionic systems with localized losses: Exact results in the hydrodynamic limit, *Phys. Rev. B* **105**, 054303 (2022).
- [32] S. Datta, *Electronic Transport in Mesoscopic Systems* (Cambridge University Press, Cambridge, 1997).
- [33] P. C. Burke, J. Wiersig, and M. Haque, Non-Hermitian scattering on a tight-binding lattice, *Phys. Rev. A* **102**, 012212 (2020).
- [34] B. Dóra, D. Sticlet, and C. P. Moca, Non-Hermitian Lindhard function and Friedel oscillations, *Phys. Rev. B* **104**, 125113 (2021).
- [35] L. Li, C. H. Lee, S. Mu, and J. Gong, Critical non-Hermitian skin effect, *Nat. Commun.* **11**, 5491 (2020).
- [36] L. Li, C. H. Lee, and J. Gong, Impurity induced scale-free localization, *Commun. Phys.* **4**, 42 (2021).
- [37] K. Yokomizo and S. Murakami, Scaling rule for the critical non-Hermitian skin effect, *Phys. Rev. B* **104**, 165117 (2021).
- [38] C.-X. Guo, X. Wang, H. Hu, and S. Chen, Accumulation of scale-free localized states induced by local non-hermiticity, *Phys. Rev. B* **107**, 134121 (2023).
- [39] Recently, we noticed that scale-free localization induced by a local loss is also discussed in Ref. [38] for a closed chain, which is consistent with our model under periodic boundary condition in the Supplemental Material [41]. However, the interplay between  $\mathcal{PT}$  symmetry breaking and boundary conditions and the subsequent criterion are not studied in Ref. [38]. Moreover, the existence of a group of exponentially localized states induced by a single impurity is not found in Ref. [38].
- [40] K. Yokomizo and S. Murakami, Non-Bloch band theory of non-Hermitian systems, *Phys. Rev. Lett.* **123**, 066404 (2019).
- [41] See Supplemental Material at <http://link.aps.org/supplemental/10.1103/PhysRevB.108.L161409> for details of calculations and more examples for local-perturbation-induced exponentially localized eigenmodes and  $\mathcal{PT}$  breaking.
- [42] K. G. Makris, R. El-Ganainy, D. N. Christodoulides, and Z. H. Musslimani, Beam dynamics in  $\mathcal{PT}$  symmetric optical lattices, *Phys. Rev. Lett.* **100**, 103904 (2008).
- [43] R. El-Ganainy, K. G. Makris, D. N. Christodoulides, and Z. H. Musslimani, Theory of coupled optical  $\mathcal{PT}$ -symmetric structures, *Opt. Lett.* **32**, 2632 (2007).
- [44] C. E. Rüter, K. G. Makris, R. El-Ganainy, D. N. Christodoulides, M. Segev, and D. Kip, Observation of parity–time symmetry in optics, *Nat. Phys.* **6**, 192 (2010).
- [45] A. Guo, G. J. Salamo, D. Duchesne, R. Morandotti, M. Volatier-Ravat, V. Aimez, G. A. Siviloglou, and D. N. Christodoulides, Observation of  $\mathcal{PT}$ -symmetry breaking in complex optical potentials, *Phys. Rev. Lett.* **103**, 093902 (2009).
- [46] B. Zhen, C. W. Hsu, Y. Igarashi, L. Lu, I. Kaminer, A. Pick, S.-L. Chua, J. D. Joannopoulos, and M. Soljačić, Spawning rings of exceptional points out of Dirac cones, *Nature (London)* **525**, 354 (2015).
- [47] K. Ding, Z. Q. Zhang, and C. T. Chan, Coalescence of exceptional points and phase diagrams for one-dimensional  $\mathcal{PT}$ -symmetric photonic crystals, *Phys. Rev. B* **92**, 235310 (2015).
- [48] A. Cerjan, A. Raman, and S. Fan, Exceptional contours and band structure design in parity-time symmetric photonic crystals, *Phys. Rev. Lett.* **116**, 203902 (2016).
- [49] I. Carusotto, D. Gerace, H. E. Tureci, S. De Liberato, C. Ciuti, and A. Imamoglu, Fermionized photons in an array of driven dissipative nonlinear cavities, *Phys. Rev. Lett.* **103**, 033601 (2009).

- [50] R. O. Umucalılar and I. Carusotto, Fractional quantum hall states of photons in an array of dissipative coupled cavities, *Phys. Rev. Lett.* **108**, 206809 (2012).
- [51] C.-E. Bardyn and A. İmamoğlu, Majorana-like modes of light in a one-dimensional array of nonlinear cavities, *Phys. Rev. Lett.* **109**, 253606 (2012).
- [52] M. C. Dartiailh, T. Kontos, B. Douçot, and A. Cottet, Direct cavity detection of Majorana pairs, *Phys. Rev. Lett.* **118**, 126803 (2017).
- [53] P. Deuar, A. Ferrier, M. Matuszewski, G. Orso, and M. H. Szymańska, Fully quantum scalable description of driven-dissipative lattice models, *PRX Quantum* **2**, 010319 (2021).
- [54] F. C. Alcaraz, M. N. Barber, M. T. Batchelor, R. J. Baxter, and G. R. W. Quispel, Surface exponents of the quantum XXZ, Ashkin-Teller and Potts models, *J. Phys. A: Math. Gen.* **20**, 6397 (1987).
- [55] H.-R. Wang, B. Li, F. Song, and Z. Wang, Scale-free non-Hermitian skin effect in a boundary-dissipated spin chain, [arXiv:2301.11896](https://arxiv.org/abs/2301.11896).